analytical chemistry

pubs.acs.org/ac Article

Ultrathin Silica Integration for Enhancing Reliability of Microfluidic Photoionization Detectors

Xiaheng Huang,[⊥] Ruchi Sharma,[⊥] Anjali Devi Sivakumar, Shuo Yang, and Xudong Fan*

Cite This: *Anal. Chem.* 2023, 95, 8496−8504 Read Online

ACCESS | Metrics & More | Article Recommendations | Supporting Information

ABSTRACT: Microfluidic photoionization detectors (μPIDs) based on silicon chips can rapidly and sensitively detect volatile compounds. However, the applications of μPID are limited by the manual assembly process using glue, which may outgas and clog the fluidic channel, and by the short lifetime of the vacuum ultraviolet (VUV) lamps (especially, argon lamps). Here, we developed a gold−gold cold welding-based microfabrication process to integrate ultrathin (10 nm) silica into μPID. The silica coating enables direct bonding of the VUV window to silicon under amicable conditions and works as a moisture and plasma exposure barrier for VUV windows that are susceptible to hygroscopicity and solarization. Detailed characterization of the silica coating was conducted, showing that the 10 nm silica coating allows 40−80% VUV transmission from 8.5 to 11.5 eV. It is further shown that the silica-protected μPID maintained 90% of its original sensitivity after 2200 h of exposure to ambient (dew point = 8.0 ± 1.8 °C), compared to 39% without silica. Furthermore, argon plasma inside an argon VUV lamp was identified as the dominant degradation source for the LiF window with color centers formation in UV−vis and VUV transmission spectra. Ultrathin silica was then also demonstrated effective in protecting the LiF from argon plasma exposure. Lastly, thermal annealing was found to bleach the color centers and restore VUV transmission of degraded LiF windows effectively, which will lead to future development of a new type of VUV lamp and the corresponding μPID (and PID in general) that can be mass produced with a high yield, a longer lifetime, and better regenerability.

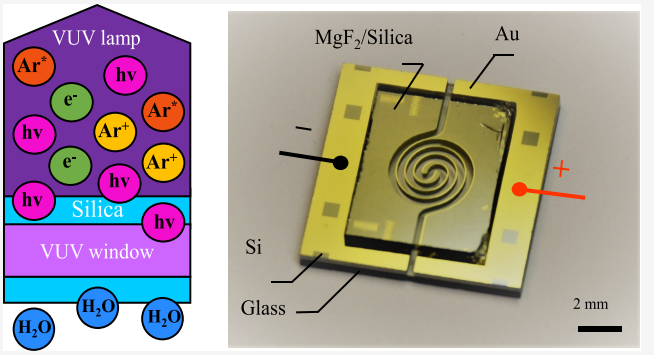

INTRODUCTION

Photoionization detectors (PIDs) are widely used for detecting volatile organic compounds (VOCs).[1−19] Benefiting from its small footprint, lamp-based PIDs have been implemented in many field applications like environmental monitoring, industrial hygiene, healthcare, *etc.*[4,18,20−29]

Conventionally, a VUV lamp is filled with low-pressure xenon (Xe, VUV photon energy up to 9.9 eV), krypton (Kr, up to 10.6 eV), or argon (Ar, up to 11.7 eV).[1,30] A MgF_2 window is used for Kr and other lamps whose photon energy is <10.6 eV (wavelength > 117 nm). However, for an Ar lamp, which emits 11.7 eV photons and can ionize VOCs whose ionization potential (IP) is >10.6 eV, a LiF window with a high transmission near 11.7 eV, needs to be used.

All these VUV windows, particularly, LiF windows, are highly susceptible to moisture (hygroscopicity)[1,15,16,19,31,32] and color center formation (solarization) caused by highly energetic ions and VUV photons.[1,33,34] While a MgF_2 window provides reliable operation over 3000 h,[1] a LiF window lasts only ∼300 h[1,15] due to higher hygroscopicity,[1,15,31,32] faster solarization,[1,33,34] and fill gas leak[1,35] resulting from the larger mismatch of the LiF thermal expansion coefficient (CTE) to the glass lamp housing.

Recently, we developed a silicon chip-based microfluidic PID (μPID),[7,14] which has fast responses and a subpicogram detection limit. However, currently, our μPID is manually assembled by pressing the lamp's bottom against the top of the microfluidic chip and then sealing the edges with glue. This process is subject to human errors that may cause gas leakage and a low yield (*e.g.*, glues may accidentally clog the channels), making the whole process not amicable to mass production. Further, the glue may outgas and produce a background signal. Therefore, it is desirable to integrate a VUV window on top of the microfluidic chip glue-free.[8] Unfortunately, most established hermetic bonding techniques (*e.g.*, eutectic, anodic, and fusion)[7,13,36] are not applicable for bonding MgF_2 or LiF with silicon, since fluoride glass is easy to crack at the high temperatures required for processing (>300 °C) due to the large thermal mismatch.

Received: January 23, 2023
Accepted: May 11, 2023
Published: May 25, 2023

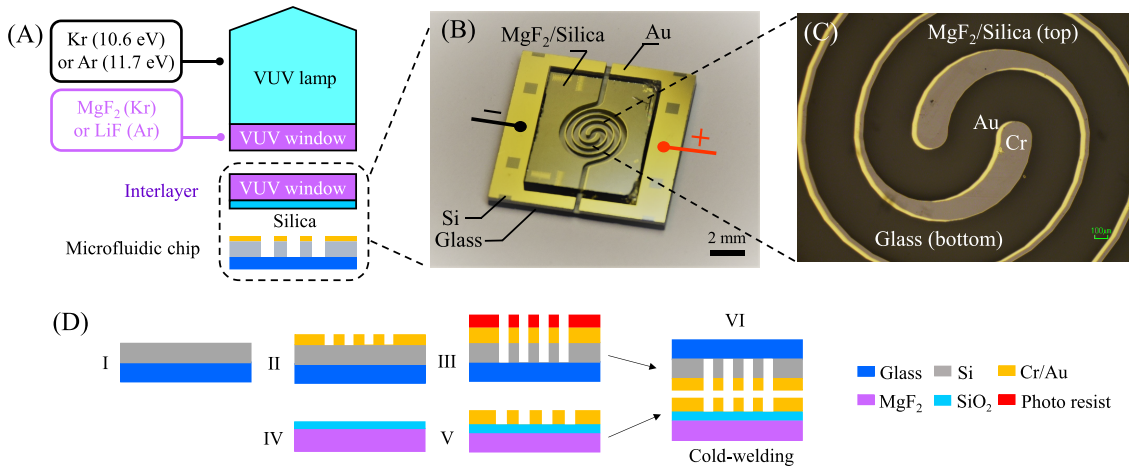

Figure 1. (A) Generic device structure of a silica-integrated photoionization detector (SIPID) consisting of a vacuum ultraviolet (VUV) lamp, an interlayer of silica-coated VUV window, and a microfluidic channel. The VUV lamps are commercially available, which come with a 1 mm-thick built-in MgF_2 and LiF window for a krypton (Kr) and argon (Ar) lamp, respectively. (B) Photograph of a microfluidic chip bonded with a 10 nm-silica-coated 0.5 mm thick MgF_2 interlayer. (C) Micrograph of the center of the spiral microfluidic channel in (B). The labeled Cr and Au are on the top MgF_2 window and the bottom silicon, respectively. (D) Microfabrication process: (I) anodic bonding; (II) e-beam evaporation and lift-off; (III) deep reactive-ion etching (DRIE); (IV) plasma-enhanced chemical vapor deposition (PECVD); (V) evaporation and Au/Cr etch; (VI) Au−Au cold-welding.

The present work is aimed at achieving (1) glue-free bonding between a VUV lamp and a silicon chip for future high-yield mass production and (2) increased lifetime of a VUV lamp and hence PID, especially an Ar-based lamp with a LiF window. Here, we demonstrated an integrated μPID with a VUV window coated with an ultrathin (10 nm) silica layer. A new microfabrication process based on cold welding was developed, enabling a silica-coated VUV window to be bonded directly on top of a silicon chip and resulting in reliable and high-yield assembly of a μPID amenable to industrial-scale production. We also found that the silica coating maintains a good VUV transmission while offering strong protection against humid environments. 40−80% of the original sensitivity (*i.e.*, without the silica coating) was achieved for the VOCs of various IPs (8.5−11.5 eV). Using silica as the moisture barrier, it is shown that the silica-protected μPID maintains 90% of its original sensitivity after 2200 h of exposure to ambient, compared to 39% without silica. We also investigated the degradation mechanisms of the LiF window in an Ar lamp, showing Ar plasma exposure as the dominant degradation source other than the commonly believed moisture effect. Furthermore, ultrathin silica was demonstrated as an effective barrier protecting LiF windows from Ar plasma, suggesting a new Ar lamp design to increase its lifetime. Finally, thermal bleaching was explored to effectively restore the VUV transmission of degraded LiF windows, providing a possible route for future design and manufacturing of regenerable VUV lamps and PIDs.

MATERIALS AND METHODS

Figure 1A shows the μPID configuration. The Si and glass wafers were cleaned using piranha solution and then anodically bonded. A 30 nm chromium (Cr)/200 nm gold (Au) was lithographically patterned and evaporated onto the silicon surface using a lift-off process. Another layer of photoresist (PR) was patterned for deep reactive-ion etching (DRIE) through the Si to form microchannels having a cross section of 390 μm (width) × 400 μm (depth), a wall thickness of 40 μm, and a length of 3.9 cm. The entire spiral channel had an overall size of 4 mm in diameter matching the VUV illumination area of a Kr lamp (Figure 1B). The wafer was then diced. Further, a predetermined thickness of SiO_2 was deposited on a MgF_2 substrate (*i.e.*, the VUV window) via plasma-enhanced vapor deposition (PECVD), which was used as an interlayer in Figure 1A. The 30 nm Cr/200 nm Au was evaporated and wet-etched with a pattern matching that of the Si microchannel. Finally, the microfluidic die and the MgF_2 die were piranha cleaned and then Au−Au cold-welded through a flip chip bonder at 150 °C and under a pressure of 2 MPa in ambient conditions for 10 min (see Figure 1C for the cold-welded interface). As shown in Figure 1B, the microfluidic die was designed larger than the MgF_2 die such that the gold electrodes on the silicon were exposed and accessible for wire bonding. Note that the microfluidic chip described above was designed for the Kr lamp assembly (*i.e.*, Kr μPID). For the Ar lamp (*i.e.*, Ar μPID), due to a larger lamp size, the spiral channel was modified and had a larger overall size of 7 mm in diameter with a length of 10 cm. For the LiF interlayer, due to the restriction of processing LiF in our cleanroom facilities, SiO_2 was sputtered on a LiF substrate, and the silica-coated LiF substrate was then mechanically fixed on the microfluidic chip using UV-curable epoxy. However, the similar microfabrication process developed for the MgF_2 interlayer is still applicable. All other materials and methods are described in the Supporting Information.

RESULTS AND DISCUSSION

Silica Integrated Microfluidic Photoionization Detector Device Structure and Fabrication. Figure 1A depicts a generic device structure of a silica-integrated microfluidic photoionization detector (SIPID). To protect the VUV window, an interlayer was formed by coating silica on the VUV window surface facing the microfluidic channel, *i.e.*, the side exposed to ambient moisture and VOC analytes during detection. The interlayer was then integrated onto the microfluidic chip through gold−gold cold-welding[37−40] using lithographically patterned gold as the intermediate adhesive layer. Note that the counter gold layer on the microfluidic chip

https://doi.org/10.1021/acs.analchem.3c00354
Anal. Chem. 2023, 95, 8496−8504

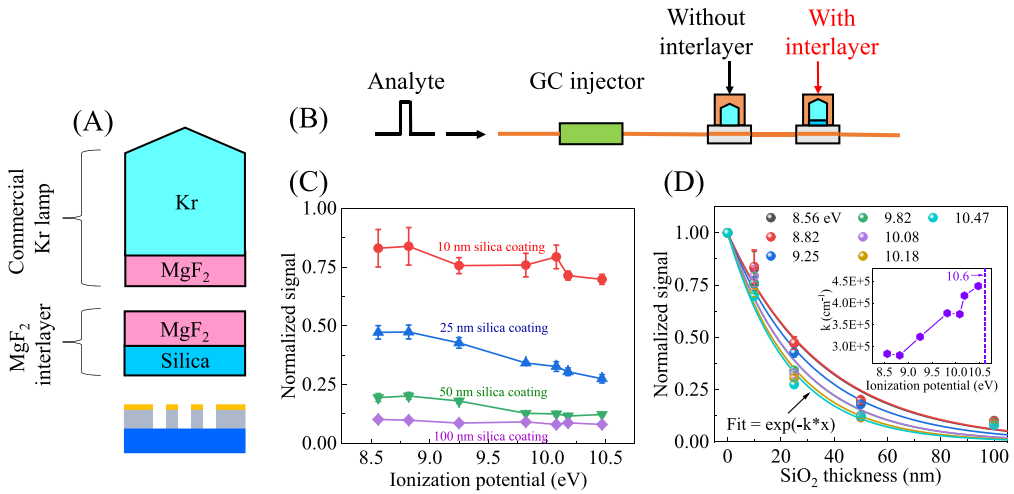

Figure 2. (A) Device structure of an SIPID using a commercial Kr lamp and a MgF_2 interlayer coated with various thicknesses (0 to 100 nm) of silica. (B) Setup used to characterize the silica VUV transmission. The analytes (see Table S1) with a range of IPs were injected via a bench-top gas chromatography (GC) injector. Two Kr-based PIDs were connected in series. The one without an interlayer was used to calibrate the signal obtained by the other one with an interlayer (*i.e.*, the device under test—DUT) coated with various thicknesses of silica. (C) Normalized signal obtained by the DUT vs IPs for different thicknesses of silica coating. The normalization is defined as the ratio of peak areas of respective analytes (with corresponding IPs) between the DUT with a silica coating and the DUT having a bare interlayer without any coating. The signal of a DUT normalized to the calibration PID is presented in Figure S1. (D) Normalized signal, which reflects the overall VUV transmission efficiency of the silica coating, extracted from (C) for different silica coating thicknesses. A single exponential function ($\exp(-k \times x)$, Beer-Lambert law) is used to fit each curve at respective IPs for extracting the corresponding pseudoabsorption coefficients. The R^2 values for the seven fits are 0.985, 0.985, 0.996, 0.985, 0.975, 0.988, and 0.988 from 8.56 to 10.47 eV. Inset: pseudoabsorption coefficient vs IP. The vertical dashed line indicates 10.6 eV. Error bars were obtained with three measurements.

also serves the electrode contacts accessible for wire bond packaging. As an example, Figure 1B,C shows a 10 nm-silica-coated MgF_2 window integrated microfluidic chip with the full microfabrication process illustrated in Figure 1D. See details in Materials and Methods.

Unlike traditional hermetic bonding methods[36] requiring high temperatures (>300 °C) for long periods (>1 h), cold welding allows for a low-temperature (150 °C) bonding process in a short time (10 min) to prevent VUV window cracking caused by the large thermal expansion coefficient (CTE) mismatch (CTE_{Si} = 2.6; CTE_{MgF2} = 13.7; CTE_{LiF} = 37; unit: 10^{-6}/K). On the other hand, compared to other low-temperature bonding techniques[41−44] (*e.g.*, polymer bonding) that cannot achieve a hermetic seal due to the gas permeable nature, the gold cold-welded interface in the SIPID provides a leak-free encapsulation that can sustain a flow rate up to 40 mL/min, sufficient for most applications in gas chromatography. It is noteworthy that, compared to manual glue bonding of individual dies, cold welding can be applied at the wafer level, resulting in increased yield and reduced cost per chip.

The commercial PID lamp, which comes with a 1 mm thick built-in VUV window (MgF_2 for a Kr lamp and LiF for an Ar lamp), was then mechanically attached on top of the integrated interlayer using glue along the lamp's edge such that both the bottom surface of the lamp's built-in VUV window and the top surface of the interlayer VUV window are sealed from ambient. Note that although the glue was still used here for simplicity and convenience, unlike our previous design,[7,14] in the current design, the VUV lamp was easily attached to the top of the interlayer and the glue was no longer in contact with the microfluidic chip beneath. Other packaging techniques[8] (*e.g.*, 3D printing) can also be employed to make a lamp fixture and completely avoid using glue. For future manufacturing, the built-in VUV window on a commercial lamp can be precoated with silica and cold-welded to the silicon microfluidic chip without using an interlayer.

Silica VUV Transmission. The silica coating on a VUV window may inevitably compromise the overall VUV transmission. Ideally, the silica coating should be ultrathin to minimize its VUV absorption; meanwhile, it should be sufficiently thick to ensure a uniform and dense coverage on the VUV window for efficiently blocking moisture permeation. To characterize the VUV transmission of the silica coating, a series of Kr lamp (10.6 eV)-based SIPIDs (see Figure 2A) were constructed with various thicknesses of silica coating (via PECVD) on the MgF_2 interlayer. As shown in Figure 2B, analytes (see Table S1) of various IPs were injected and then detected by two Kr-based PIDs connected in series. The first PID did not have an interlayer and was used to calibrate the downstream SIPIDs (*i.e.*, the device under test - DUT) due to the nondestructive and flow-through nature of our PID.[7]

Figure S1A shows the peak area detected by the DUT normalized to that detected by the calibration PID for the analytes of different IPs. The interlayers in the DUT had various silica coating thicknesses ranging from 0 (*i.e.*, just a bare 0.5 mm MgF_2 window) to 100 nm. In Figure 2C, the VUV transmission of the silica coating can be extracted by further normalizing the peak area in Figure S1A to that obtained with the 0 nm silica coating. It is found that a 10 nm silica coating retained 70−80% of the original sensitivity (*i.e.*, 70−80% overall VUV transmission). In general, with the increased silica coating thickness, the sensitivity for the analytes with lower IPs (*e.g.*, 8.56 and 8.82 eV) decays more slowly than for those with higher IPs (*e.g.*, 10.18 and 10.47 eV), as shown in the inset of Figure 2D. This can be explained as follows. First, the Kr-lamp has multiple VUV photon emission energies with the highest being 10.6 eV.[30] The analytes with lower IPs can be ionized (and subsequently

https://doi.org/10.1021/acs.analchem.3c00354
Anal. Chem. 2023, 95, 8496−8504

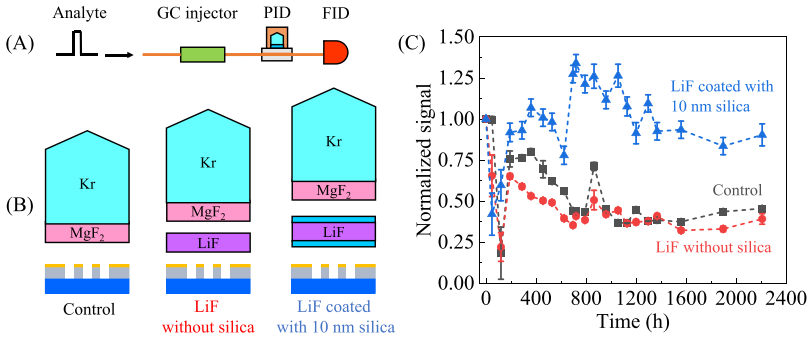

Figure 3. (A) Setup for PID lifetime characterization. An FID, assumed to have no degradation, was connected downstream to the PID as the calibration detector. (B) Kr lamp based PIDs for lifetime test − (1) control PID without any interlayer (*i.e.*, the Kr lamp was directly placed and sealed on the top of the microfluidic chip); (2) PID with a bare LiF interlayer; (3) PID with a LiF interlayer coated with 10 nm silica on both sides. Note that only the bottom surface of the interlayer was exposed to microfluidic channels and hence the ambient environment. The top surface was sealed by surrounding UV-epoxy, which is assumed to have no water vapor coming from outside. (C) Signal over aging time obtained by the three devices in (B). The signals from each device are normalized to its relative sensitivity (*i.e.*, PID/FID) at the 0th hour. The PIDs were aged in ambient environment (see Figure S4). The signal of the PIDs was periodically measured using benzene. The Kr lamps and the FID were turned off without carrier gas during aging intervals. Error bars were obtained with three measurements.

detected) by not only 10.6 eV photons but also the emitted photons with other lower energies. In contrast, the analytes with high IPs (*e.g.*, 10.18 and 10.47 eV) can only be ionized by 10.6 eV photons. Furthermore, silica's VUV absorption increases with increased VUV photon energy (*i.e.*, decreased VUV photon wavelength) in the range of 8.5−10.5 eV.[45−47] Consequently, the detection of analytes having lower IPs is less impacted by the silica coating than that of those having IPs closer to 10.6 eV (see the inset in Figure 2D). The pseudoabsorption coefficient of the silica coating at 10.6 eV is estimated to be 4.5×10^5 cm^{-1} by using the decay curve of the analyte with 10.47 eV IP in Figure 2D and a single exponential curve fit (*i.e.*, Beer-Lambert law), in general agreement with the previous studies that show an absorption coefficient of 6×10^5 cm^{-1} at 10.6 eV[46,47] for silica. Note that only the analyte whose IP is close to 10.6 eV can be used to extract the silica absorption coefficient at 10.6 eV since only 10.6 eV photons can ionize it, as discussed previously.

Furthermore, to ensure uniform coverage of an ultrathin 10 nm silica coating on the MgF_2 window, the surface morphology of bare and 10 nm-silica-coated MgF_2 windows was examined using atomic force microscopy (AFM). The surface roughness remained the same before (RMS = 0.9 nm) and after (RMS = 0.8 nm) silica coating (see Figure S2), suggesting a pin-hole free ultrathin silica layer on MgF_2.

We also explored the PECVD silicon nitride coating due to its reported better performance as a moisture barrier[48−50] than silica. Only 50% of the original sensitivity was obtained for a 10 nm-thick coating of silicon nitride (Figure S1B). Metallic coatings such as a thin film consisting of sputtered Cr (2.5 nm)/Au (2.5 nm) were previously reported that allowed for >50% VUV transmission on an MgF_2 window,[15] but they have questionable moisture protection effectiveness due to the discontinuous and island-like surface typically formed by ultrathin metals.[51,52] In addition, a thin metal coating is not applicable in the current μPID design as it would short the silicon electrodes of the microfluidic chip underneath.

The VUV transmission of the silica coating beyond 10.6 eV was further investigated using Ar lamps (with the highest emission energy of 11.7 eV) and LiF windows with a similar device structure, *i.e.*, replacing Kr lamps (MgF_2 interlayer) with Ar lamps (LiF interlayer). Due to restrictions on processing LiF in our cleanroom facility, silica could only be sputtered on the LiF substrates instead of using PECVD. In Figure S3A, 10 nm sputtered silica shows 40−60% of original sensitivity (*i.e.*, overall VUV transmission) for the analytes with the IP of 8.5−11.5 eV. The ∼20% discrepancy compared to a PECVD coating is likely caused by the extrinsic VUV transmission loss of the host LiF substrate due to its exposure to Ar plasma[34,53−55] during the sputtering process, as evidenced by the LiF color center formation after sputtering (see Figure S3B).

Ultrathin Silica as the Moisture Barrier. The reliability of PIDs was tested using the setup in Figure 3A. An FID was connected downstream in series with the PID and used as the calibration detector assuming no degradation. The relative sensitivity of the PID under test is defined as the ratio of peak areas of PID over FID. The reliability of the PID was evaluated using the time evolution of its relative sensitivity under certain aging conditions.

To examine the silica protection on VUV windows against moisture, we designed a hybrid device architecture of SIPID in which the more hygroscopic LiF window (with or without silica) was selected as the interlayer exposed to ambient to amplify the moisture effect (since MgF_2 window is less susceptible to moisture), and the Kr lamp was employed as the VUV source due to its known superior robustness to an Ar lamp. Therefore, other possible degradation mechanisms of an Ar lamp (see the discussion later) could be ruled out and the VUV light source was deemed stable throughout the test. As shown in Figure 3B, two SIPIDs (one with a bare LiF interlayer and the other with a 10 nm silica double-coated LiF interlayer) and a control device without an interlayer were tested. Note that the 10 nm silica coating on the top LiF interlayer surface was for precaution only, which was essentially unnecessary as its perimeter was sealed by UV-epoxy that has a very low water vapor transmission rate. The PIDs were aged in ambient with a temperature of 19.7 ± 0.7 °C and a relative humidity of 41.5 ± 10.4%, corresponding to a dew point = 8.0 ± 1.8 °C that is close to the annual average value recorded at Detroit Metro Airport station in Michigan[56] (see Figure S4). The signal (*i.e.*, relative sensitivity) of the PIDs was periodically measured using benzene (IP = 9.2 eV). Between two consecutive measurements (*i.e.*, during an aging

https://doi.org/10.1021/acs.analchem.3c00354
Anal. Chem. 2023, 95, 8496−8504

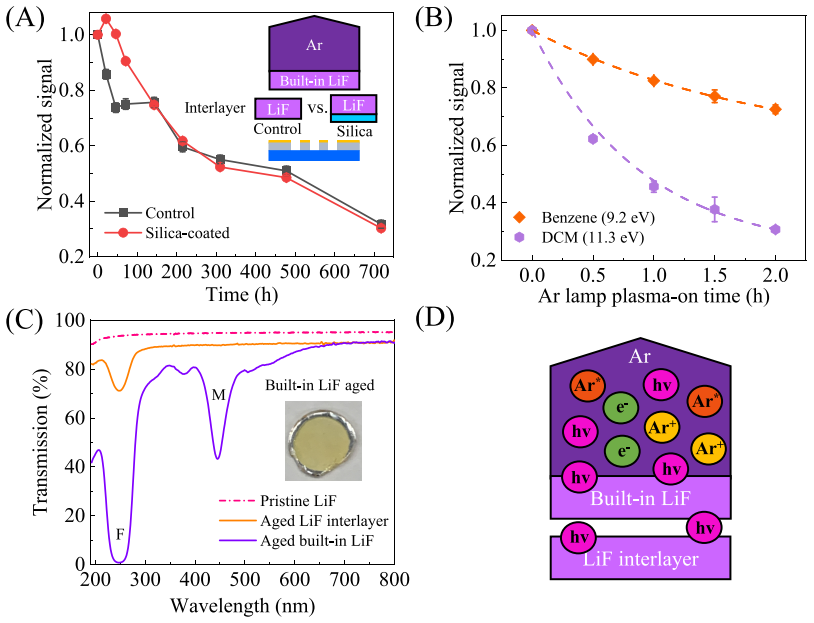

Figure 4. (A) Signal of Ar-SIPIDs (with and without silica) for heptane vs time. The signals from each device are normalized to its relative sensitivity at the 0th hour. Inset: Ar lamp-based SIPIDs (Ar-SIPID) with (1) bare LiF interlayer as a control and (2) silica-coated (10 nm) LiF interlayer. The normalized signals for two other analytes, toluene and dichloromethane (DCM), are shown in Figure S6B. The aging protocol was the same as in Figure 3C that the plasma was only turned on during each measurement point. (B) Normalized signal of another Ar-SIPID in continuous operation (*i.e.*, the Ar lamp was turned on throughout the aging experiment) vs aging time for benzene and DCM. Dashed lines are the fitting curves of a single exponential decay function ($A \times \exp(-k \times x) + C$). The exponential decay constants are $k = 0.53$ and $1.14\ h^{-1}$ for benzene and DCM, respectively. A and C are fitting constants. (C) Transmission spectra of pristine LiF, aged interlayer LiF, and aged built-in LiF. F and M refer to the F color center and M color center, respectively. The aged interlayer and the built-in LiFs were dissembled from the 700 h aged control Ar-SIPID (*i.e.*, without silica). The inset shows a photo of the dissembled aged built-in LiF window. (D) Illustration of different degradation agents generated by argon plasma and their exposure to built-in and interlayer LiF windows.

cycle), the PIDs were not in operation with the Kr lamp (*i.e.*, plasma) and carrier gas being turned off.

Figure 3C shows the moisture reliability of the three devices. During the initial 50−100 h, all three devices underwent a significant drop in sensitivity, which recovered after 200 h. Although the exact cause of this anomaly is unknown, we speculate that it may be attributed to an initial "burn-in" phase of the μPID. The silica-coated LiF device maintained its sensitivity at 90% after 2200 h of aging. In comparison, both the control device and bare LiF device have degraded to 45 and 39%, respectively, with the same aging time. We observed that the bare LiF device underwent the fastest degradation among the three devices in the first 800 h, after which the sensitivity plateaued at ∼40%. The control device (*i.e.*, the one with a built-in MgF_2 window only) shared a similar trend reaching the 40% plateau with a slower degradation rate. The results suggest that the LiF window experiences faster degradation when exposed to ambient than the MgF_2 window (control), while the eventual VUV transmission loss after a long term is similar for both windows. In contrast, the silica-coated LiF window (or interlayer) shows no obvious degradation trend with only 10% VUV loss when sensitivity plateaued, attesting to the effective moisture protection of the 10 nm silica coating.

To understand the role of silica as the moisture barrier, X-ray photoelectron spectroscopy (XPS) depth profiling was performed to examine the moisture degradation mechanism of LiF. As shown in Figure S5A, it was found that the chemical compositions of both fresh and aged LiF substrates (*i.e.*, exposed to ambient for 1000 h) stayed almost constant from the top surface to 200 nm deep into the bulk. Consistently, the binding energy of the Li 1s level also remained relatively unchanged from surface to bulk (see Figure S5B). These results suggest that LiF crystals remained chemically unaltered even when exposed to a moisture dosage that had caused significant loss in VUV transmission. A previous study showed that LiF experienced significantly increased surface roughness when exposed to humidity,[32] suggesting that the VUV transmission loss may be due to the stronger surface scattering. Therefore, ultrathin silica acts as a barrier to prevent moisture from being in contact with LiF and as a surface passivation layer to maintain the morphology of the LiF surface.

Study of Ar Based SIPID. We next implement the ultrathin silica integration to the LiF interlayers in the Ar lamp-based SIPIDs (Ar-SIPID), as shown in the inset of Figure 4A, to examine whether Ar lamp lifetime could be improved. Figure 4A demonstrates the moisture reliability test of control and silica-coated Ar-SIPIDs. The aging protocol was the same as previously described in Figure 3. Surprisingly, both devices degraded almost identically over 700 h of aging regardless of silica protection. Compared to the results using the Kr lamps in Figure 3C, Ar-SIPIDs' sensitivity had a faster degradation rate without plateauing. In addition, it was visually observed that the built-in LiF windows in both Ar lamps of the tested Ar-SIPIDs appeared yellowish just after ∼50 h of aging (see Figure S6A), and such yellowish discoloration was manifested throughout the whole bulk crystal of LiF. All evidence suggests that there are new degradation mechanisms in the Ar lamp itself that are faster than the moisture-induced degradation discussed previously.

The major new degradation source turns out to be the Ar plasma generated inside the Ar lamp. To decouple its impact

https://doi.org/10.1021/acs.analchem.3c00354
Anal. Chem. 2023, 95, 8496−8504

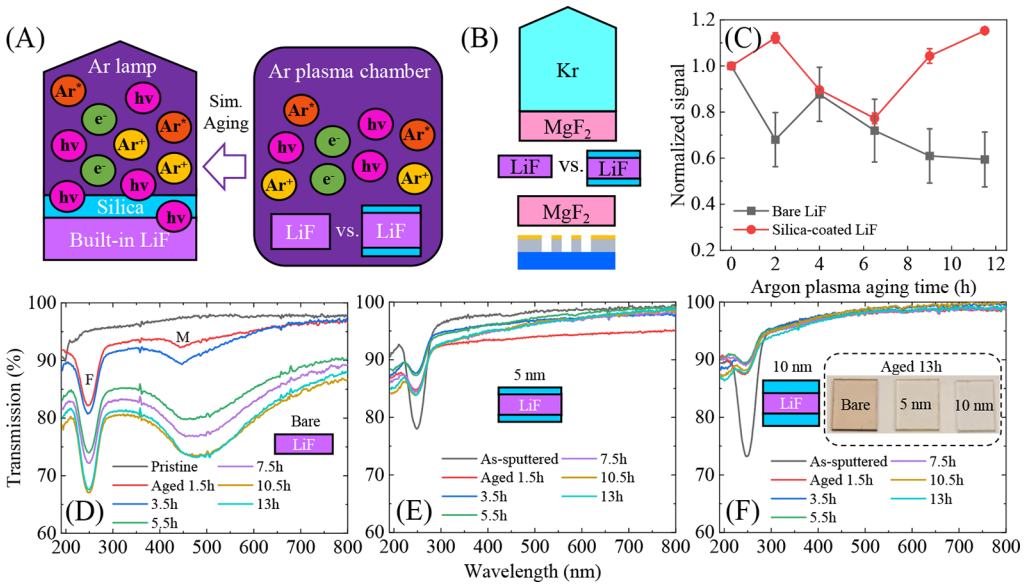

Figure 5. (A) Simulating Ar plasma aging. (Left) Conceptual design of an Ar lamp with silica coating on built-in LiF facing inward. (Right) The aging effects in an argon-lamp setting illustrated on the left were simulated by placing (1) bare and (2) silica-coated LiF interlayers inside an argon plasma chamber. The Ar plasma aging setup is described in Figure S7A. (B) Device structure for testing VUV degradation of bare and silica-coated LiF interlayers after they were aged in an argon plasma chamber in (A). During the test, a stretchable tape was used to sandwich the LiF interlayer between the Kr lamp and the microfluidic chip with a MgF_2 interlayer. After each test, the LiF interlayer was disassembled and placed back in the argon plasma chamber for further aging. (C) Normalized signal of the device in (B) with respect to the argon plasma aging time for both bare and silica-coated LiF interlayer (10 nm coated on both sides) using benzene as the analyte. The signal is normalized to the relative sensitivity obtained at the 0th hour for each interlayer. The normalized signals for heptane are shown in Figure S7B. The testing protocol is the same as shown in Figure 3. Error bars were obtained with three measurements. (D−F) Transmission spectra of a bare and silica-coated LiF (5 and 10 nm on both sides) interlayer at different Ar plasma aging times. Note that the as-sputtered LiF substrates develop initial 250 nm color centers due to exposure to Ar plasma during the sputtering process. Inset in (F) shows the photos of aged samples of bare, 5 nm silica-coated, and 10 nm silica-coated LiF. F and M in (D) refer to the F color center and the M color center, respectively.

from the moisture reliability test performed before, another control device (*i.e.*, Ar-SIPID without silica) was constructed and it was aged with Ar plasma being turned on continuously. As evidenced in Figure 4B, with constant Ar plasma aging, the Ar-SIPID demonstrated an accelerated exponential-like decay, taking only 2 h to drop to 75 and 30% for benzene (IP = 9.2 eV and dichloromethane (DCM, IP = 11.3 eV), respectively. In addition, the yellowish discoloration of the built-in LiF window has also developed (not necessarily requiring 2 h). Such results indicate that the dominant aging of Ar-SIPIDs in Figure 4A could be attributed to the accumulated short-term (approximately 30 min) Ar plasma exposure when it was turned on during the measurements at each aging test time point. Additionally, as seen in Figure S6B, throughout 700 h of moisture aging, the sensitivity loss for DCM is faster than toluene (IP = 8.8 eV) and heptane (10.1 eV, Figure 4A), consistent with the trend observed in Figure 4B with accelerated Ar plasma exposure, that is, the sensitivity decays faster for the analytes whose IPs are closer to the maximum emitted photon energy of Ar plasma (11.7 eV), as discussed in Figure 2D for the Kr plasma case.

To better understand the degradation mechanism of the LiF windows in the Ar-SIPID, the built-in LiF window as well as the interlayer LiF window were dissembled from the 700 h aged control Ar-SIPID (*i.e.*, without silica) for further characterizations. From the transmission spectra in Figure 4C, the aged built-in LiF window shows two dominant signature color centers of LiF (labeled as F and M), which render its yellowish appearance as seen in the inset of Figure 4C. These color center formations result from high energy irradiations[34,53−55,57] (*e.g.*, X-rays, Extreme UV (EUV), VUV, heavy ions, protons, electrons, *etc.*). Opposite to the significantly deteriorated built-in LiF window, the directly contacted LiF interlayer underneath only developed a small F center without any visual discoloration, indicative of different degradation mechanisms. As illustrated in Figure 4D, the built-in LiF window was directly exposed to all four species generated by Ar plasma inside the lamp body—(1) Ar*: argon excited state; (2) Ar^+: argon ion; (3) e^-: electron; and (4) *hv*: VUV photon (*e.g.*, 11.7 eV). In contrast, the LiF interlayer was only subject to the VUV photons transmitted through the built-in window. The above comparison suggests that the combination of Ar excited states, Ar ions, and electrons might play a more detrimental role to the LiF than VUV photons. However, it is also worth noting that the dose of VUV photons (hence the damage) incident on the LiF interlayer is lower than that on the native built-in LiF window during aging, especially after the built-in window became yellowish. Indeed, a similar effect was observed previously when a VUV-transmissive indium thin film was coated on the LiF substrate exposed to Ar discharge.[54] It was found that the ratios of the initial slopes of the decay curves (*i.e.*, VUV transmission of the LiF) closely matched the ratios of the initially transmitted intensities determined by the thickness of the indium thin film.

Ultrathin Silica as the Ar Plasma Protective Layer. The fact that the LiF interlayer suffered only mild degradation from Ar plasma with the shielding of the built-in window described in the previous section suggests a rational design to eventually integrate an ultrathin dielectric (*e.g.*, silica) coating on the inner surface of the built-in LiF window in an Ar lamp

https://doi.org/10.1021/acs.analchem.3c00354
Anal. Chem. 2023, 95, 8496−8504

as depicted in Figure 5A. Unlike vulnerable LiF, silica is not susceptible to any color center formation and has one of the lowest sputtering yields of any standard materials when exposed to Ar plasma (meaning that silica can withstand Ar plasma very well). Combined with its decent transmission in VUV as described before, ultrathin silica becomes a promising candidate to protect LiF from Ar plasma.

Limited by the inability to build an actual Ar lamp in-house, we performed Ar plasma aging on the bare and silica-coated LiF substrates using a commercial Ar plasma chamber, which simulated the actual environment inside an Ar lamp as illustrated in Figure 5A. After aging in the plasma chamber, the LiF substrates were inserted as an additional interlayer into a Kr lamp-based PID device, as illustrated in Figure 5B, to extract the VUV transmission loss. Once again, we used a Kr lamp (instead of an Ar lamp) to provide a stable VUV source, as discussed previously. In addition, a stretchable tape instead of UV-epoxy was used for easy removal of the assembled VUV lamp and the interlayer between two consecutive aging cycles. The overall VUV transmission loss is hence inferred as the said PID sensitivity loss, assuming that other components in the stack (*i.e.*, the Kr lamp and MgF_2 interlayer) stayed intact.

In Figure 5C, the 10 nm silica-coated LiF substrate remained stable (with a 15% increase in fact) after 11.5 h of exposure to Ar plasma. In contrast, the bare LiF decreased to 60% of its original VUV transmission for the same aging. Figure 5D−F presents the UV−vis spectra obtained simultaneously with another batch of substrates, showing that bare LiF progressively developed the F and M color centers with overall transmission loss, resulting in visual discoloration after 13 h of aging (see the inset in Figure 5F). In contrast, the silica-coated LiF substrates showed an initial F color center as-sputtered, which in fact partially recovered after the first 1.5 h of aging, and the overall transmission stayed relatively stable without developing any other new color centers. Compared to small fluctuations in the transmission spectra of the 5 nm silica-coated LiF substrate, the 10 nm sample presents an almost constant overall transmission during aging. As mentioned before, the initial F color center of the silica-coated samples is caused by the sputtering process using Ar plasma (see Figure S3B), as further evidenced by the lower transmission value of the F center (wavelength: 250 nm) in 10 nm coating (0.73) than that of 5 nm (0.78). Note that the phenomenon of an initial partial recovery of the F center is consistent with the small increase of the VUV transmission observed in Figure 5C, which also occurred right after the first 2 h of aging. Such color center healing could be attributed to the UV bleaching effect[55,58] by the UV photons inside the Ar plasma chamber.

The above proof-of-concept experiments using an Ar plasma chamber suggest that ultrathin silica effectively prevents VUV transmission loss and color center formation in LiF from plasma exposure and thus can potentially be integrated on the inner surface (*i.e.*, facing plasma) of a LiF (and MgF_2[34,59]) window to increase the Ar (and Kr) lamp lifetime. In contrast, other VUV transmissive thin films, such as indium[54] and gold,[15] are not applicable because their metallic nature would disrupt the dielectric environment for dielectric-barrier-discharge plasma to form inside a VUV lamp. Lastly, we found that the transmission of the degraded LiF windows can be restored (*i.e.*, bleached) by thermal annealing. The details are described in Figures S8−S11.

CONCLUSIONS

We developed a microfabrication process that bonds VUV window with silicon under amicable conditions, paving the way for directly integrating VUV lamps onto μPIDs for future high yield mass production. The ultrathin silica coating was shown to be an effective barrier for both moisture and plasma exposure with good VUV transmission. The silica coating used in this work was prepared by widely employed deposition techniques (*i.e.*, PECVD and sputtering) without further processing. More advanced techniques (*e.g.*, atomic layer deposition) could potentially offer superior quality silica coatings to further enhance the performance. In the future, more robust VUV lamps with enhanced lifetime can be developed by coating ultrathin silica on both sides of the VUV window—the outer silica layer for moisture protection and the inner for plasma shielding. Such a new type of VUV lamp and the corresponding PID will significantly reduce the maintenance effort in field applications under harsh environments and broaden the detection range of VOCs beyond 10.6 eV (Kr-based PID) by using a reliable Ar-based PID (up to 11.7 eV).

ASSOCIATED CONTENT

Supporting Information

The Supporting Information is available free of charge at https://pubs.acs.org/doi/10.1021/acs.analchem.3c00354.

IPs for all compounds used in the tests; additional device characterization methods and results, including schematics and photographs of experimental setups; and restoration of aged LiF windows by thermal and DUV bleaching (PDF)

AUTHOR INFORMATION

Corresponding Author

Xudong Fan − *Department of Biomedical Engineering, Center for Wireless Integrated MicroSensing and Systems (WIMS2), and Max Harry Weil Institute for Critical Care Research and Innovation, University of Michigan, Ann Arbor, Michigan 48109, United States;* orcid.org/0000-0003-0149-1326; Email: xsfan@umich.edu

Authors

Xiaheng Huang − *Department of Biomedical Engineering, Department of Electrical Engineering and Computer Science, Center for Wireless Integrated MicroSensing and Systems (WIMS2), and Max Harry Weil Institute for Critical Care Research and Innovation, University of Michigan, Ann Arbor, Michigan 48109, United States;* orcid.org/0000-0002-0960-1211

Ruchi Sharma − *Department of Biomedical Engineering, Center for Wireless Integrated MicroSensing and Systems (WIMS2), and Max Harry Weil Institute for Critical Care Research and Innovation, University of Michigan, Ann Arbor, Michigan 48109, United States*

Anjali Devi Sivakumar − *Department of Biomedical Engineering, Department of Electrical Engineering and Computer Science, Center for Wireless Integrated MicroSensing and Systems (WIMS2), and Max Harry Weil Institute for Critical Care Research and Innovation, University of Michigan, Ann Arbor, Michigan 48109, United States*

https://doi.org/10.1021/acs.analchem.3c00354
Anal. Chem. 2023, 95, 8496−8504

Shuo Yang − *Department of Biomedical Engineering, Center for Wireless Integrated MicroSensing and Systems (WIMS2), and Max Harry Weil Institute for Critical Care Research and Innovation, University of Michigan, Ann Arbor, Michigan 48109, United States*

Complete contact information is available at: https://pubs.acs.org/10.1021/acs.analchem.3c00354

Author Contributions

⊥X.H. and R.S. contributed equally to this work.

Notes

The authors declare the following competing financial interest(s): The photoionization detector (PID) technology used in the article is licensed to Nanova Environmental, Blu Biotech, and ChromX Health. X.F. is a co-inventor of this technology and has financial interest in the above companies. He also serves as a paid or unpaid consultant to these companies.

■ ACKNOWLEDGMENTS

The authors acknowledge the support from National Institute for Occupational Safety and Health (NIOSH) via R01 OH011082-01A1, National Institutes of Health (NIH) via U01TR004066, and the Office of the Director of National Intelligence (ODNI), Intelligence Advanced Research Projects Activity (IARPA), via IARPA FA8650-19-C-9101. The views and conclusions contained herein are those of the authors and should not be interpreted as necessarily representing the official policies or endorsements, either expressed or implied, of the ODNI, IARPA, or the U.S. Government. The U.S. Government is authorized to reproduce and distribute reprints for governmental purposes notwithstanding any copyright annotation thereon. The authors acknowledge the Lurie Nanofabrication Facility for aid in microfabrication, the Battery Lab for the sputtering process, Zhongrui Li from Electron Microbeam Analysis Lab for aid in X-ray diffraction measurement, and Nancy Muyanja in the Center for Materials Characterization for aid in XPS measurement.

■ REFERENCES

(1) Haag, W.; Wrenn, C. *The PID Handbook-Theory and Applications of Direct-Reading Photoionization Detectors (PIDs)*, 2nd.; RAE Systems Inc.: San Jose, CA; 2006.
(2) Freedman, A. N. *J. Chromatogr. A* **1980**, *190*, 263−273.
(3) Driscoll, J. N. *J. Chromatogr.* **1977**, *134*, 49−55.
(4) Driscoll, J. N.; Duffy, M. *Chromatography* **1987**, *2*, 21−27.
(5) Verner, P. *J. Chromatogr. A* **1984**, *300*, 249−264.
(6) Coelho Rezende, G.; Le Calvé, S.; Brandner, J. J.; Newport, D. *Sens. Actuators, B* **2019**, *287*, 86−94.
(7) Zhu, H.; Nidetz, R.; Zhou, M.; Lee, J.; Buggaveeti, S.; Kurabayashi, K.; Fan, X. *Lab Chip* **2015**, *15*, 3021−3029.
(8) Rezende, G. C.; Le Calvé, S.; Brandner, J. J.; Newport, D. *Micromachines* **2019**, *10*, 228−239.
(9) Zhu, H.; Zhou, M.; Lee, J.; Nidetz, R.; Kurabayashi, K.; Fan, X. *Anal. Chem.* **2016**, *88*, 8780−8786.
(10) Akbar, M.; Shakeel, H.; Agah, M. *Lab Chip* **2015**, *15*, 1748−1758.
(11) Narayanan, S.; Rice, G.; Agah, M. *Microchim. Acta* **2014**, *181*, 493−499.
(12) Narayanan, S.; Rice, G.; Agah, M. *Sens. Actuators, B* **2015**, *206*, 190−197.
(13) Li, M. W.-H.; Ghosh, A.; Sharma, R.; Zhu, H.; Fan, X. *Sens. Actuators, B* **2021**, *332*, No. 129504.
(14) Li, M. W.-H.; Ghosh, A.; Venkatasubramanian, A.; Sharma, R.; Huang, X.; Fan, X. *ACS Sens.* **2021**, *6*, 2348−2355.
(15) Miranda, A.; De Beule, P. A. A. *Sensors* **2021**, *21*, 7738.
(16) Xu, W.; Cai, Y.; Gao, S.; Hou, S.; Yang, Y.; Duan, Y.; Fu, Q.; Chen, F.; Wu, J. *Sens. Actuators, B* **2021**, *330*, No. 129285.
(17) Rezende, G. C.; Le Calvé, S.; Brandner, J. J.; Newport, D. *Sens. Actuators, B* **2020**, *324*, No. 128667.
(18) You, D. W.; Seon, Y. S.; Jang, Y.; Bang, J.; Oh, J. S.; Jung, K. W. *J. Chromatogr. A* **2020**, *1625*, No. 461267.
(19) Soo, J.-C.; Lee, E. G.; LeBouf, R. F.; Kashon, M. L.; Chisholm, W.; Harper, M. *J. Occup. Environ. Hyg.* **2018**, *15*, 351−360.
(20) Cavalcante, R. M.; de Andrade, M. V. F.; Marins, R. V.; Oliveira, L. D. M. *Microchem. J.* **2010**, *96*, 337−343.
(21) Bocos-Bintintan, V.; Smolenschi, A.; Ratiu, I. A. *Stud. Univ. Babes-Bolyai, Chem.* **2016**, *61*, 203−212.
(22) Jia, M. Y.; Koziel, J.; Pawliszyn, J. *Field Anal. Chem. Tech.* **2000**, *4*, 73−84.
(23) Qin, Y.; Gianchandani, Y. B. *Microsyst. Nanoeng.* **2016**, *2*, 15049.
(24) Lee, J.; Sayler, S. K.; Zhou, M.; Zhu, H.; Richardson, R. J.; Neitzel, R. L.; Kurabayashi, K.; Fan, X. *Anal. Methods* **2018**, *10*, 237−244.
(25) Sharma, R.; Zhou, M.; Hunter, M. D.; Fan, X. *J. Agric. Food Chem.* **2019**, *67*, 7530−7537.
(26) Zhou, M.; Sharma, R.; Zhu, H.; Li, Z.; Li, J.; Wang, S.; Bisco, E.; Massey, J.; Pennington, A.; Sjoding, M.; Dickson, R. P.; Park, P.; Hyzy, R.; Napolitano, L.; Gillies, C. E.; Ward, K. R.; Fan, X. *Anal. Bioanal. Chem.* **2019**, *411*, 6435−6447.
(27) Huang, X.; Li, M. W.-h.; Zang, W.; Huang, X.; Sivakumar, A. D.; Sharma, R.; Fan, X. *Microsyst. Nanoeng.* **2022**, *8*, 1−12.
(28) Sharma, R.; Zhou, M.; Tiba, M. H.; McCracken, B. M.; Dickson, R. P.; Gillies, C. E.; Sjoding, M. W.; Nemzek, J. A.; Ward, K. R.; Stringer, K. A.; Fan, X. *ERJ Open Res.* **2022**, *8*, 00154.
(29) Sharma, R.; Zang, W.; Tabartehfarahani, A.; Lam, A.; Huang, X.; Sivakumar, A. D.; Thota, C.; Yang, S.; Dickson, R. P.; Sjoding, M. W.; Bisco, E.; Mahmood, C. C.; Diaz, K. M.; Sautter, N.; Ansari, S.; Ward, K. R.; Fan, X. *JAMA Network Open* **2023**, *6*, e230982−e230982.
(30) Huffman, R. E.; Larrabee, J. C.; Tanaka, Y. *Appl. Opt.* **1965**, *4*, 1581−1588.
(31) Fleming, B.; Quijada, M.; Hennessy, J.; Egan, A.; Del Hoyo, J.; Hicks, B. A.; Wiley, J.; Kruczek, N.; Erickson, N.; France, K. *Appl. Opt.* **2017**, *56*, 9941.
(32) Lewis, D. M.; Plewe, C. M.; Gallion Stapley, A.; Vawdrey, J. J.; Turley, R. S.; Allred, D. D. *Proc. SPIE* **2020**, *11451*, 1145141.
(33) Dunn, M.; Nemechek, J. J.; Tienvieri, C. T. *Lasers Optronics* **1989**, *8*, 59−64.
(34) Reft, C. S.; Becher, J.; Kernell, R. L. *Appl. Opt.* **1980**, *19*, 4156−4158.
(35) Mulder, B. *J. Phys. E: Sci. Instrum.* **1977**, *10*, 591.
(36) Cunningham, S. J.; Kupnik, M. *Wafer Bonding*; Springer US: 2011; pp. 817−877, DOI: 10.1007/978-0-387-47318-5_11.
(37) Ferguson, G. S.; Chaudhury, M. K.; Sigal, G. B.; Whitesides, G. M. *Science* **1991**, *253*, 776−778.
(38) Lu, Y.; Huang, J. Y.; Wang, C.; Sun, S.; Lou, J. *Nat. Nanotechnol.* **2010**, *5*, 218−224.
(39) Higurashi, E.; Okumura, K.; Kunimune, Y.; Suga, T.; Hagiwara, K. *IEICE Trans. Electron.* **2017**, *E100.C*, 156−160.
(40) Yamamoto, M.; Matsumae, T.; Kurashima, Y.; Takagi, H.; Suga, T.; Itoh, T.; Higurashi, E. *Micromachines* **2019**, *10*, 119.
(41) Kim, H.; Najafi, K. *J. Microelectromech. Syst.* **2005**, *14*, 1347−1355.
(42) Niklaus, F.; Stemme, G.; Lu, J.-Q.; Gutmann, R. J. *J. Appl. Phys.* **2006**, *99*, No. 031101.
(43) Noh, H.-s.; Moon, K.-s.; Cannon, A.; Hesketh, P. J.; Wong, C. P. *J. Micromech. Microeng.* **2004**, *14*, 625.
(44) Satyanarayana, S.; Karnik, R. N.; Majumdar, A. *J. Microelectromech. Syst.* **2005**, *14*, 392−399.
(45) Philipp, H. R. *J. Phys. Chem. Solids* **1971**, *32*, 1935−1945.

(46) Tan, G. L.; Lemon, M. F.; Jones, D. J.; French, R. H. *Phys. Rev. B* **2005**, *72*, No. 205117.
(47) Kitamura, R.; Pilon, L.; Jonasz, M. *Appl. Opt.* **2007**, *46*, 8118−8133.
(48) Cho, T.-Y.; Lee, W.-J.; Lee, S.-J.; Lee, J.-H.; Ryu, J.; Cho, S.-K.; Choa, S.-H. *Thin Solid Films* **2018**, *660*, 101−107.
(49) Lin, H.; Xu, L.; Chen, X.; Wang, X.; Sheng, M.; Stubhan, F.; Merkel, K.-H.; Wilde, J. *Thin Solid Films* **1998**, *333*, 71−76.
(50) Robles, S.; Yieh, E.; Nguyen, B. C. *J. Electrochem. Soc.* **1995**, *142*, 580.
(51) Doron-Mor, I.; Barkay, Z.; Filip-Granit, N.; Vaskevich, A.; Rubinstein, I. *Chem. Mater.* **2004**, *16*, 3476−3483.
(52) Axelevitch, A.; Gorenstein, B.; Golan, G. *Phys. Procedia* **2012**, *32*, 1−13.
(53) Kato, R.; Nakashima, S.-i.; Nakamura, K.; Uchida, Y. *J. Phys. Soc. Jpn.* **1960**, *15*, 2111−2112.
(54) Warneck, P. *J. Opt. Soc. Am.* **1965**, *55*, 921−925.
(55) Kaufman, J.; Clark, C. *J. Chem. Phys.* **1963**, *38*, 1388−1399.
(56) https://www.ncei.noaa.gov/products/land-based-station/local-climatological-data. Last accessed May 9, 2023
(57) Schwartz, K.; Trautmann, C.; El-Said, A. S.; Neumann, R.; Toulemonde, M.; Knolle, W. *Phys. Rev. B* **2004**, *70*, No. 184104.
(58) Mador, I. L.; Wallis, R. F.; Williams, M. C.; Herman, R. C. *Phys. Rev.* **1954**, *96*, 617.
(59) Kolopus, J. L.; Lewis, J. T.; Unruh, W. P.; Nelson, L. G. *J. Phys. C: Solid State Phys.* **1971**, *4*, 3007.

https://doi.org/10.1021/acs.analchem.3c00354
Anal. Chem. 2023, 95, 8496−8504